

Synthesis of piperazine functionalized magnetic sporopollenin: a new organic-inorganic hybrid material for the removal of lead(II) and arsenic(III) from aqueous solution

Naqhiyah Farhan Ahmad¹ · Muhammad Afzal Kamboh^{1,2} · Hamid Rashidi Nodeh^{1,3} · Siti Nadiah Binti Abd Halim¹ · Sharifah Mohamad^{1,4}

Received: 4 December 2016 / Accepted: 24 July 2017 / Published online: 3 August 2017
© Springer-Verlag GmbH Germany 2017

Abstract The present work describes the successful functionalization/magnetization of bio-polymeric spores of *Lycopodium clavatum* (sporopollenin) with 1-(2-hydroxyethyl) piperazine. Analytical techniques, i.e., Fourier transform infrared (FT-IR), field emission scanning electron microscope (FESEM), energy-dispersive X-ray spectroscopy (EDS), and vibrating sample magnetometer (VSM), were used to confirm the formation of 1-(2-hydroxyethyl) piperazine-functionalized magnetic sporopollenin (*MNPs-Sp-HEP*). The proposed adsorbent (*MNPs-Sp-HEP*) was used for the removal of noxious Pb(II) and As(III) metal ions from aqueous media through a batch-wise method. Different experimental parameters were optimized for the effective removal of selected noxious metal ions. Maximum adsorption capacity (q_m) 13.36 and 69.85 mg g⁻¹ for Pb(II) and As(III), respectively, were obtained. Thermodynamic parameters such as free energy (ΔG°), entropy (ΔS°), and enthalpy (ΔH°) were also studied from the adsorption results and were used to elaborate the mechanism of their confiscation. The obtained results indicated that newly adsorbent can be successfully applied for the decontamination of noxious Pb(II) and As(III) from the aqueous environment.

Keywords Sporopollenin · Piperazine · Magnetization · Pb(II) and As(III) · Adsorption isotherm · Thermodynamic · Kinetic

Introduction

Recently, industrial sectors discharge a huge amount of effluents which contains variety of highly toxic as well as persistent pollutants such as dyes, phenols, pesticides, and heavy metals (Liu et al. 2010; Sáez et al. 2014; He 2015; Meenakumari and Philip 2015; Vymazal and Brezinova 2015; Bakhshaei et al. 2016; Shahabuddin et al. 2016). The release of the untreated effluents to the natural stream is of great anxiety because due to rapidly growing urbanization and industrialization, the scale of contaminated effluents is escalating day by day. Industrial units like battery manufacturing and metal pleating and finishing are renowned for the Pb(II) and As(III) contamination (Gupta and Rastogi 2008). Exposure of Pb(II) to the natural aqueous environment as a result of different anthropogenic activities such as industrialization, mining, and agriculture is becoming alarming form last few decades (Cheng et al. 2015; He 2015). The toxicity of Pb(II) can triggered to brain damage, mental deficiency, anemia, and behavioral problem if inhaled or swallowed (Gupta and Rastogi 2008). Due to the high toxicity of the Pb(II), the World Health Organization (WHO) has set maximum residual level 10 ng mL⁻¹ in water samples (WHO 2008; Edition 2011). As(III) is also an omnipresent eco-toxin; its presence in aqueous media victimizes the huge amount of masses throughout the world (Tyrovola et al. 2007; Ali 2012). Its short-term exposure brings about dermal, respiratory, gastrointestinal, cardiovascular, mutagenic, and carcinogenic effects while chronically lead to hyper- and hypo-pigmentation, lungs, bladder and kidney cancer, nausea, neurological

Responsible editor: Guilherme L. Dotto

✉ Sharifah Mohamad
sharifahm@um.edu.my

- ¹ Department of Chemistry, Faculty of Science, University Malaya, 50603 Kuala Lumpur, Malaysia
- ² Department of Chemistry, Shaheed Benazir Bhutto University, Shaheed Benazirabad, Sindh, Pakistan
- ³ Department of Chemistry, Faculty of Science, University of Tehran, Tehran, Iran
- ⁴ University of Malaya Center for Ionic Liquids, University of Malaya, 50603 Kuala Lumpur, Malaysia

disorders, muscular weakness, and loss of appetite (Gohari et al. 2013; Tang et al. 2013). In this regard, European Union (EU) and WHO set $0.001 \mu\text{g L}^{-1}$ as an extreme contamination level for As(III) in drinking water (Community 1998; WHO 2008). Thus, precise monitoring, determination, and remediation of noxious Pb(II) and As(III) metal ions from aqueous environment is extremely important for human health.

Therefore, it is very important to develop a new technique that is able to remove and reduce the concentration of Pb(II) and As(III) in aqueous environment to permitted levels. There are numerous technologies have been studied for low-cost and more effective to remove heavy metals such as chemical precipitation, ion exchange, adsorption, and membrane separation (Dabrowski et al. 2004; Fadzil et al. 2016; Swamalatha and Ayoob 2016; Vilela et al. 2016). Among these methods, adsorption has become one of the alternative treatments in current years, since it can effectively remove various toxic metals as the course of convenient design and operation (Swarnalatha and Ayoob 2016; Vilela et al. 2016). Furthermore, adsorption process is simple, easy, and convenient approach to deal with metal-contaminated effluents (Barakat 2011).

Different types of materials have been used for adsorption approaches such as activated carbon, silica-based materials, polymers, and biomass (Aguado et al. 2009; Ucar et al. 2014; Jain et al. 2015; Lapwanit et al. 2016). For adsorption process, structure of adsorbent plays an important role in order to enhance mechanical, chemical, and thermal stability. Biopolymeric spores of *Lycopodium clavatum* (sporopollenin) possess tremendous mechanical, thermal, and chemical stability. Additionally sporopollenin due the high content of functional groups can be easily functionalized/magnetized (Paunov and Stoyanov 2007). Numerous modifications on the surface of sporopollenin have been stated by various researchers (Çimen et al. 2014; Kamboh et al. 2016; Şener et al. 2016).

To obtain selective adsorption of Pb(II) and As(III), amine functionalized adsorbents are considered as eminent and was previously reported (Georgiou et al. 2016; Nonkumwong et al. 2016). According to Pearson acid base concept (HSAB), this functional groups show higher selectivity toward both selected metals. In addition, iron oxide nanoparticles are capable to treat enormous amounts of wastewater in a short period and also can be easily separated from wastewater (Ibrahim et al. 2015a, b). The specific characteristics of iron oxide nanoparticles provide a convenient tool for exploring magnetic separation techniques (Ibrahim et al. 2015a). The higher surface area offered by magnetic particles has improved the adsorption behavior compared to that of the raw bio-sorbent (Sureshkumar and Daniel 2016). Magnetically modified bio-sorbent reveal promising adsorption capacity toward mixed wastewaters (Sivashankar et al. 2014).

In current study, the sporopollenin was modified with 3-cyanopropyltrimethoxysilane (CPTS) and functionalized with 1-(2-hydroxyethyl) piperazine (*Sp-HEP*). The functionalized sporopollenin was magnetized with iron oxide nanoparticles (*MNPs-Sp-HEP*). The combination of amine ligand and iron oxide nanoparticles with sporopollenin enhanced the adsorption properties of sporopollenin and resulting in strong binding affinities toward selected target pollutants. The synthesized of *MNPs-Sp-HEP* was successfully used for the removal of Pb(II) and As(III) ions from aqueous solution. The adsorption kinetics was examined using the pseudo-first-order, pseudo-second-order, and intraparticle diffusion equations and the equilibrium data fitted with two isotherm equations (Langmuir and Freundlich). The thermodynamic parameters (ΔG° , ΔH° , and ΔS°) were also calculated.

Experiment

Chemicals

All chemicals used were analytical grade and were used as received. 1-(2-Hydroxyethyl) piperazine (HEP), 3-cyanopropyltriethoxysilane (CPTS), and sporopollenin (Sp) were purchased from Sigma-Aldrich (Steinheim, Germany). $\text{FeCl}_3 \cdot 6\text{H}_2\text{O}$, $\text{FeCl}_2 \cdot 4\text{H}_2\text{O}$, 30% ammonia solution, and toluene were purchased from R&M Chemicals.

Instruments

An inductively coupled plasma–mass spectrometer (ICP-MS; Agilent 7500A series, Agilent Technologies, Palo Alto, CA, USA) was applied for determination of the heavy metals in this work. The surface morphology of the *MNPs-Sp-HEP* was determined at 2.0 kV using a JSM-6390 field emission-scanning electron microscope (FE-SEM) from JEOL (Tokyo, Japan). The FT-IR spectrum was obtained using ATR technique on a Spectrum 400 PerkinElmer in the range of $4000\text{--}450 \text{ cm}^{-1}$ with diamond as a detector. The magnetic property was tested using a vibration sample magnetometer (VSM) model 9600 (Quantum Design Inc., San Diego, USA). Magnetization measurements were carried out in an external field of up to 15 kOe at room temperature.

Synthesis of functionalized magnetic sporopollenin

3-Cyanopropyltriethoxysilane-modified sporopollenin (*CPTS-Sp*) was prepared according to the previously reported method (Çimen et al. 2014). Ten-gram sporopollenin was suspended in 67 mL dry toluene and 6 mL of CPTS was added. The mixture was then refluxed for 72 h and dried under vacuum. Herein, the functionalization as well as

magnetization of *CPTS-Sp* with *HEP* and Fe_3O_4 , respectively, in order to obtain a new *MNPs-Sp-HEP* (Fig. 1) is reported for the first time.

Functionalization of CPTS-modified Sp with HEP

Five grams of freshly prepared *Sp-CPTS* was added to 25% (v/v) of *HEP* solution and stirred at room temperature for 15 h. The residue was filtered and washed with deionized water. The *Sp-HEP* was then dried under vacuum at 80 °C for 20 h.

Magnetization of Sp-HEP (MNPs-Sp-HEP)

Five grams of $\text{FeCl}_3 \cdot 6\text{H}_2\text{O}$, 7.5 g of $\text{FeCl}_2 \cdot 4\text{H}_2\text{O}$, 2 mL 5 M HCl, 15 mL distilled water, and 2 mL ethanol was mixed in a 100-mL flask. The mixture was heated until the salt was complete dissolved. In 10 mL of solution, 0.3 g *Sp-HEP* was dispersed and stirred for 2 h at room temperature. Then, *Sp-HEP* was filtered. Immediately, it was washed with distilled water and hurriedly transferred into 1 M ammonia solution. Magnetic sporopollenin-functionalized HEP (Fig. 1) was stirred for 2 h at room temperature before collected by external magnet and washed thoroughly with distilled water (Kamboh and Yilmaz 2013).

Adsorption experiment

The adsorption efficiency of synthesized *MNPs-Sp-HEP* for Pb(II) and As(III) metal ions has been examined through adsorption procedure. The experiments were conducted into Erlenmeyer flasks (50 mL) which contain specific dosage (10–60 mg) of the adsorbent at different concentrations, i.e., 5–100 mg L^{-1} of adsorbate (aqueous solution of Pb(II) and As(III) metal ions). Finally, following the magnetic separation, residual concentration of Pb(II) and As(III) metal ions in the solution was measured by inductively coupled plasma mass spectrometry (ICP-MS) (Fig. 2). The adsorption capacity of synthesized *MNPs-Sp-HEP* and % extraction of Pb(II) and As(III) ions was calculated using Eqs. (1) and (2), respectively.

$$q_e = \frac{V(C_0 - C_e)}{m} \quad (1)$$

where q_e is the adsorption capacity (mg g^{-1}), V is the aqueous volume (L), m is the adsorption dosage (mg), and C_e (mol L^{-1}) and C_0 (mol L^{-1}) are the residual and initial concentrations of the Pb(II) and As(III) ions in the solution, respectively.

The percent efficiency (%E) of Pb(II) and As(III) ions were calculated using Eq. (2):

Fig. 1 Schematic routes for the preparation of 1-(2-hydroxyethyl) piperazine-functionalized magnetic sporopollenin (*MNPs-Sp-HEP*)

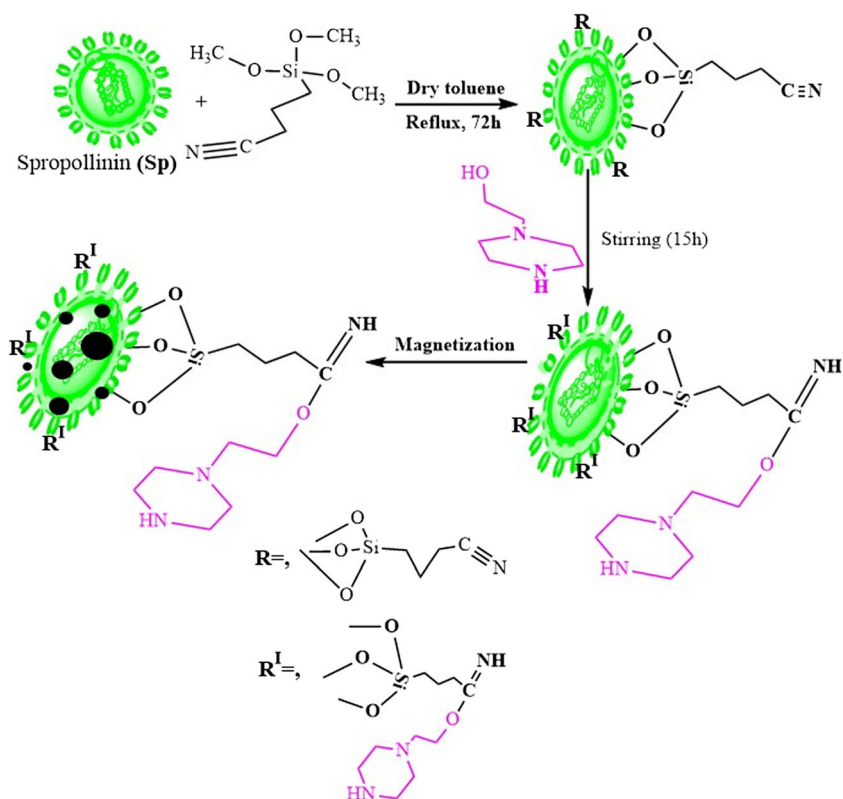
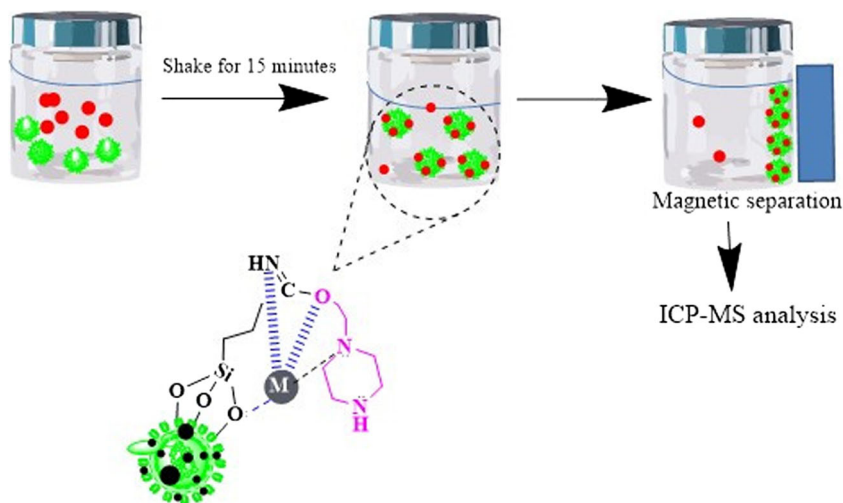


Fig. 2 Schematic procedures for removal of Pb(II) and As(III) ions by using *MNPs-Sp-HEP*



$$\%E = \frac{C_0 - C_e}{C_0} \times 100 \tag{2}$$

desorption cycle, regeneration of *MNPs-Sp-HEP* was washed thoroughly with deionized water.

Desorption and regeneration studies

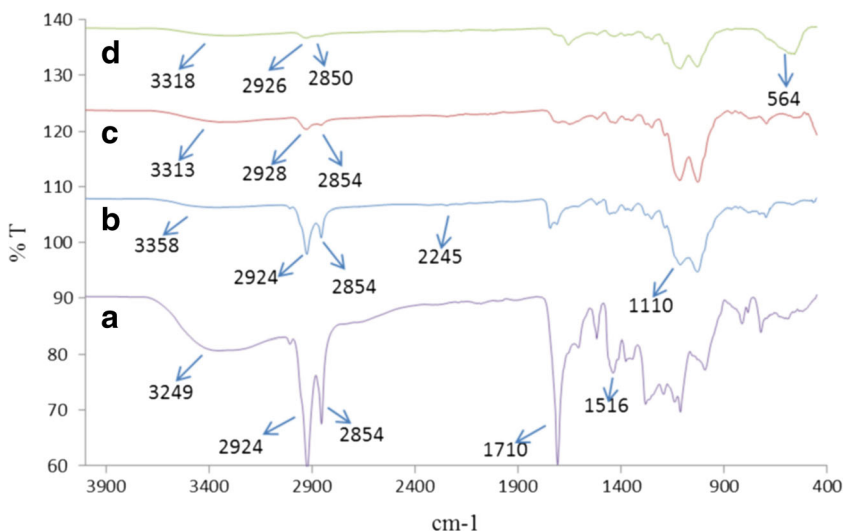
To evaluate the reusability of the adsorbent, adsorption of analytes (Pb(II) and As(III)) and regeneration of Pb-loaded *MNPs-Sp-HEP* and As-loaded *MNPs-Sp-HEP* were performed in seven consecutive cycles. In each cycle, 10 mg L⁻¹ analytes (Pb(II) and As(III)) in 10 mL of solution was mixed with 15 mg *MNPs-Sp-HEP* for 15 min. The *MNPs-Sp-HEP* was separated magnetically, and the supernatant was subjected to Pb(II) and As(III) measurements. The resultant Pb- and As-loaded sorbent was mixed with 10 mL of 0.1 M HNO₃ solution for 5 min. Prior to the next adsorption-

Results and discussion

Synthesis

The main objective of this study was to design a new organic-inorganic hybrid sporopollenin-based magnetic material with having heterocyclic core as well as amino functional groups and exploration of its extraction properties toward the selected Pb(II) and As(III) ions. To achieve the desired goal, sporopollenin was modified with 3-cyanopropyltriethoxysilane. In second step, heterocyclic core/amino functionality was achieved by the functionalization of *CPTS-Sp* with *HEP* in the presence of dry toluene. In order to acquire the hybrid/magnetic nature,

Fig. 3 FT-IR spectra of raw sporopollenin (a), *Sp-CPTS* (b), *Sp-HEP* (c), and *MNPs-Sp-HEP* (d)



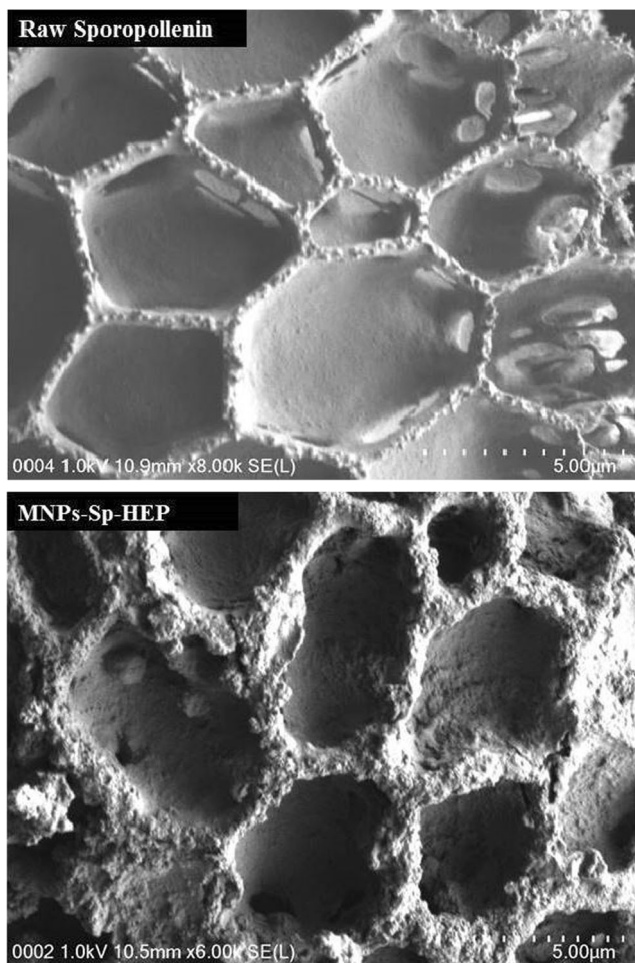


Fig. 4 FESEM images of raw sporopollenin and *MNPs-Sp-HEP*

the *Sp-HEP* was functionalized with Fe_3O_4 and the resultant hybrid *MNPs-Sp-HEP* was chosen as precursor.

Characterization

FT-IR spectral analysis

The FT-IR spectra of the functionalized sporopollenin are shown in Fig. 3a–d. The spectrum of raw sporopollenin (Fig. 3a) shows the characteristic adsorption bands of hydroxyl groups (OH), a broadband ranging from

Table 1 EDS result of functionalization of sporopollenin

Element	Sp	Sp-CPTS	Sp-HEP	<i>MNPs-Sp-HEP</i>
C	73.25	69.41	76.79	58.76
O	26.75	23.58	16.68	25.52
N		2.02	4.45	3.55
Si		4.99	2.05	2.59
Fe				9.57

3200 to 3400 cm^{-1} . The peaks at 2924 and 2854 cm^{-1} were due to C–H symmetric and a symmetric stretching, respectively. The peak shown at 1516 cm^{-1} was due to the C = C stretching vibration of the aromatic rings, and the one at 1710 cm^{-1} was due to the C = O stretching vibration of a carboxylic group (Dyab et al. 2016). The spectrum of *CPTS*-modified sporopollenin (Fig. 3b) shows the characteristic adsorption bands of cyano group (C \equiv N) and siloxane (Si–O–Si) group stretching at 2245 and 1110 cm^{-1} , respectively. The lower intensity of carboxylic group stretching in *CPTS*-modified sporopollenin (Fig. 3b) as compared to the raw sporopollenin (Fig. 3a) might be due to the modification process, and it is due to the attachment of *CPTS* on hydroxyl and carboxylic group (Fig. 3b). Frequency of OH stretching vibration in *Sp-CPTS* is shifted to 3358 from 3249 cm^{-1} (*Sp*) (Çimen et al. 2014). The successful functionalization of *Sp-CPTS* with *HEP* can be explain on the bases of disappearance as well as shifting of some diagnostic stretching bands in IR spectrum of *Sp-HEP* (Fig. 3c). Disappearance of cyano group (C \equiv N) in *Sp-HEP* spectrum (Fig. 3c) confirms that *HEP* was functionalized with the cyano group (C \equiv N), and it is a qualitative evidence for the conversion of cyano group (C \equiv N) into (C = N) group. The frequency of secondary amine from *HEP* was observed at range of 3313–3318 cm^{-1} overlapping with OH functional group from sporopollenin (Fig. 3c). The peaks at 3249 and 1710 cm^{-1} in sporopollenin (Fig. 3a) decreased drastically after immobilization of *CPTS* shows that the attachment of *CPTS* on hydroxyl and carboxylic group (Fig. 3b) and after functionalized with *HEP* shift to 1647 cm^{-1} due to presence of amine (Fig. 3c). Moreover, the sharp peak at 564 cm^{-1} may be attributed to nanoparticles (Fe_3O_4) groups obtained when *Sp-HEP* was coated with Fe_3O_4 (Fig. 3d) (Arora et al. 2016).

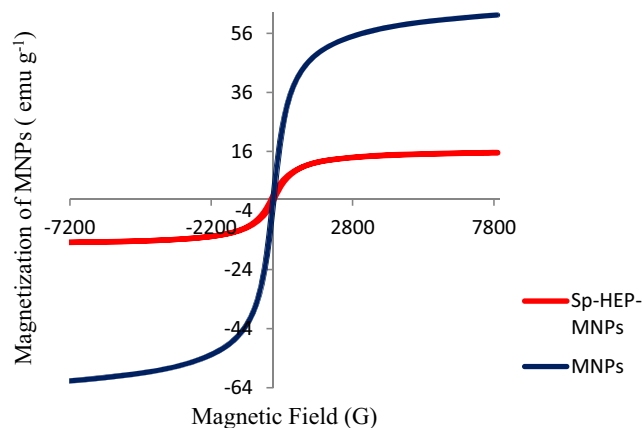


Fig. 5 The magnetic behavior of *MNPs* (blue) and *MNPs-Sp-HEP* (red)

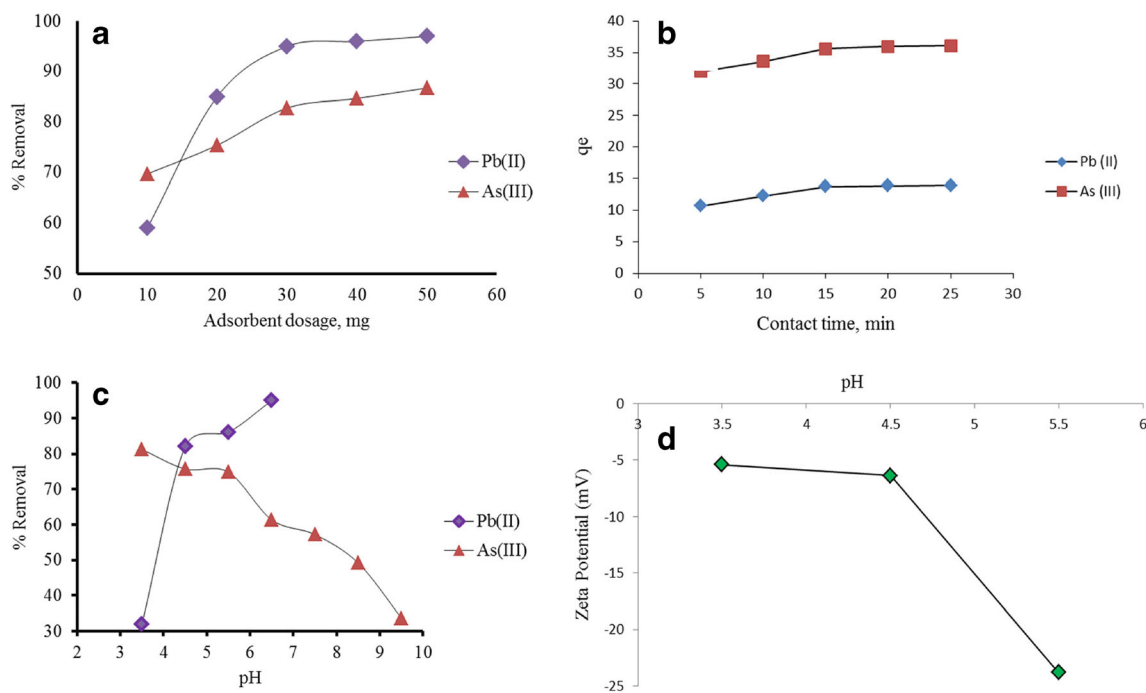


Fig. 6 The effect of dosage (a), time (b), pH (c) on the sorption of Pb(II) and As(III) ions, and the zeta potential of *MNPs-Sp-HEP* at various pHs (d)

Field emission scanning electron microscopy

The morphology images of pure sporopollenin and *MNPs-Sp-HEP* (Fig. 4) revealed that raw sporopollenin consists of an interconnected uniform hexagonal shape with pore structure (in the form of round microcapsule). The open and uniform pore structure of modified sporopollenin showed an irregular pattern due to the functionalization/magnetization with *HEP* and Fe_3O_4 , respectively, non-uniformly deposited inside the openings and on the walls. It can be seen from Fig. 4 that each pore of sporopollenin remained hollow even after modification, functionalization, and magnetization process.

Energy-dispersive spectroscopy

The pureness and elemental composition of sporopollenin and functionalized sporopollenin were investigating using EDS. The functionalized sporopollenin was compared with raw sporopollenin. Table 1 shows the elemental composition for raw sporopollenin, *Sp-CPTS*, *Sp-HEP*, and *MNPs-Sp-HEP*. The presence of additional nitrogen, silica, and iron on functionalized sporopollenin show that they are successfully functionalized/magnetize onto sporopollenin as the natural composition of sporopollenin spores are only form hydrogen, carbon, and oxygen.

VSM analysis

Magnetic properties were characterized by measuring the hysteresis and remanence curves by means of VSM. Figure 5 shows the magnetization curves of Fe_3O_4 and *MNPs-Sp-HEP*. The two curves show similar symmetrical about the origin shape which exhibits the characteristic feature of superparamagnetism. The Fe_3O_4 achieved a saturation magnetization value of 63.3 emu g^{-1} similar to that obtained from literature (Baharin et al. 2016). After functionalized with *Sp-HEP*, the saturation magnetization value dropped significantly (15.64 amu g^{-1}). This was predicted due to the coating contribution from a non-magnetic functionalized sporopollenin. However, the decreases of saturation magnetization give no significant difference

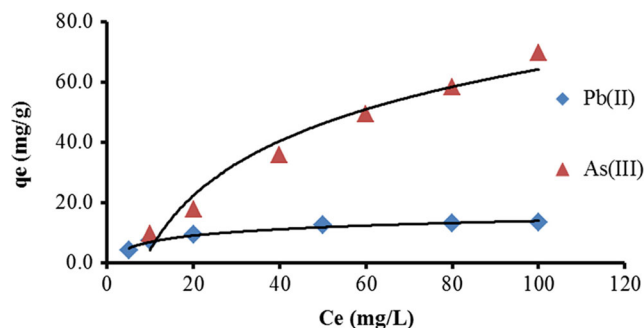


Fig. 7 Equilibrium adsorption capacities for Pb(II) and As(III) sorption using *MNPs-Sp-HEP* as adsorbent

between the two superparamagnetic properties of MNPs which is sufficient for magnetic separation with a conventional magnet (Zheng et al. 2014).

Optimization of effective parameters on removal of Pb(II) and As(III) ions

Adsorbent dosage

Figure 6a displays the influence of the adsorbent mass on the removal of target analytes. This is due to the importance of adsorbent amount in adsorption efficiency removal from water samples. Five different amounts of *MNPs-Sp-HEP* (10–50 mg) were used for the adsorption of 10 ppm of Pb(II) from 10 mL deionized water samples. The adsorption efficiencies of Pb(II) and As(III) are directly proportional to the mass of adsorbent due to an increase in adsorption sites, and thus, more analyte can occupy these sites. Beyond the 25 mg of the adsorbent dosage, there is no significant increase and adsorbent becomes almost constant. The result indicated that *MNPs-Sp-HEP* has reached the adsorption equilibrium, where the maximum capacity of the adsorbent was reached. Consequently, 25 mg was selected for the subsequent experiments.

Effect of pH

The pH of the solution plays an important role in the adsorption characteristics of Pb(II) and As(III). Figure 6c displays the removal of Pb(II) and As(III) at different pH values. The increase of the pH of the solution up to pH 6.5 increased the percentage removal of Pb(II) ions due to the electrostatic interaction between Pb(II) and negatively charged surfaces (Fig. 6d). Significant 95% was acquired at pH 6.5. The lower percentage removal of Pb(II) at low pH might be due to the competition between Pb^{2+} and H^+ with active sites and repulsion of Pb^{2+} and protonated amine. Meanwhile, the percentage removal of As(III) is optimum from pH 3.5 to 5.5. After this point, based on zeta potential result (Fig. 6d)

Fig. 8 Langmuir isotherms of removal of Pb(II) and As(III) by *MNPs-Sp-HEP*

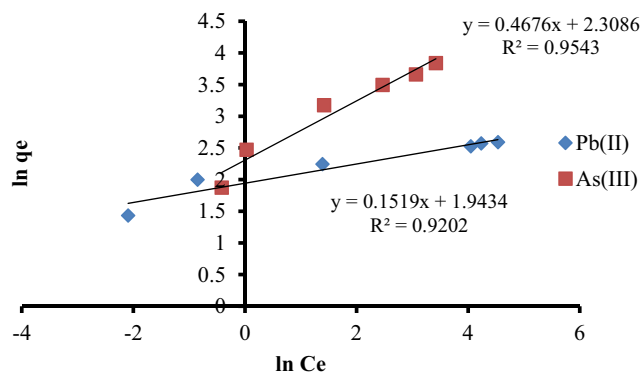
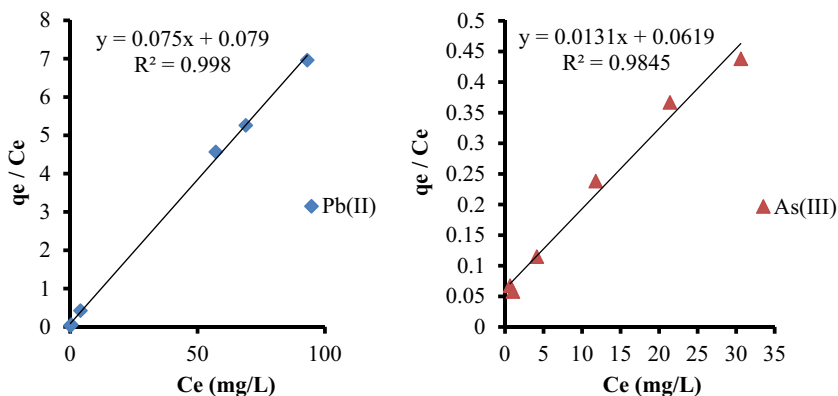


Fig. 9 Freundlich isotherms of removal of Pb(II) and As(III) by *MNPs-Sp-HEP*

at higher pH, surface of the adsorbent become more negatively charged due to deprotonation of C = N and acidic group of particle surfaces (Binks et al. 2011). Hence, the percentage removal of As(III) was decreased due to repulsion between dominant species of As(III), $H_2AsO_3^-$, and negatively charged surfaces.

Effect of contact time

Figure 6b shows the effect of the adsorption time on the removal of Pb(II) and As(III) ions. As predicted, as the contact time increase, the percent of removal for the both metal ions also increase until reached steady state values. In this study, the rapid uptake kinetics can be attributed to the hydroxyl group and nitrogen unit of nitrile and amine group from *HEP*. Thus, 15 min was enough to remove both metal ions and selected for further analysis of Pb(II) and As(III).

Adsorption isotherm

Optimization the design of an adsorption process is importance to study the interaction of adsorbate with adsorbents (adsorption isotherms). Adsorption study was carried out using different concentrations of Pb(II) and As(III) (5–

Table 2 Langmuir and Freundlich model constants and coefficient of determination for adsorption of Pb(II) and As(III) on *MNPs-Sp-HEP*

Isotherms	Equation	Isotherm constant	Pb(II)	As(III)
Langmuir				
Linear	$\frac{C_e}{q_e} = \frac{C_e}{q_m} + \frac{C_e}{q_m K_L}$	R^2 q_m K_L	0.9745 11.92 4.35	0.9747 75.19 0.24
Non-linear	$q_e = q_m K_L \frac{C_e}{1 + C_e K_L}$			
Freundlich				
Linear	$Ln q_e = Ln K_F + \frac{1}{n} Ln C_e$	R^2 K_F $1/n$	0.9202 6.98 0.1519	0.9543 15.09 0.4676
Non-linear	$q_e = K_F C_e^{1/n}$			

100 mg L⁻¹) at pH 5.5 (Fig. 7). When the concentrations of Pb(II) and As(III) were increased, q_e also increased until it reached equilibrium at higher concentrations since at high concentration adsorption sites were saturated. The adsorption mechanism of Pb(II) and As(III) on *MNPs-Sp-HEP* was studied by using adsorption models, namely, Langmuir and Freundlich.

The Langmuir model was established to represent chemisorption which assumes a monolayer deposition on a surface with a finite number of identical sites. The equation is valid for a homogenous surface (Chou et al. 2011). Therefore, at equilibrium, a saturation point is reached where no further adsorption can occur (Fig. 7). The non-linear expression of Langmuir isotherm is represented by the following equation:

$$q_e = q_m K_L \frac{C_e}{1 + C_e K_L} \tag{3}$$

where q_e is the corresponding adsorption capacity, C_e is the equilibrium ion concentration in the solution, q_m is the adsorption capacity, and K_L is the energy or net enthalpy. The plot of q_e vs. C_e for the sorption is plotted (Fig. 7).

The non-linear expression of Freundlich isotherm model is an empirical equation that describes the heterogenous adsorption energies on the adsorbent

surface (Fadzil et al. 2016), and multilayer adsorption is controlled by physisorption (i.e., van der Waal’s interaction), which can be written as

$$q_e = K_F C_e^{1/n} \tag{4}$$

where K_F and n are the Freundlich constants related to the adsorption capacity and adsorption intensity, respectively; q_e is the equilibrium solute concentration on adsorbent; and C_e is the equilibrium concentration of the solute. According to Eq. (4), the plot of q_e vs. C_e is plotted (Fig. 7).

Linear forms of the isotherms models are also widely adopted to determine the isotherm parameters or the most fitted model for the adsorption system due to the mathematical simplicity. The linear form of Langmuir is expressed as

$$\frac{C_e}{q_e} = \frac{C_e}{q_m} + \frac{1}{q_m b} \tag{5}$$

where q_e is the amount of solute sorbed on the surface of the sorbent, C_e is the equilibrium ion concentration in the solution, q_m is the maximum surface density at

Table 3 Thermodynamic parameters for sorption of Pb(II) and As(III) of *MNPs-Sp-HEP*

Target analyte	Temperature (K)	ΔG° (kJ mol ⁻¹)	ΔH° (kJ mol ⁻¹)	ΔS° (J mol ⁻¹ K ⁻¹)
Pb(II)	293	-2.73	-47.47	0.17
	303	-4.12		
	313	-6.16		
As(III)	293	-2.38	-63.46	0.22
	303	-5.34		
	313	-6.86		

Table 4 Kinetic modeling constants and coefficient of determination for adsorption of Pb(II) and As(III) on *MNPs-Sp-HEP*

Model/isotherm constant	Equation/value for Pb(II)	Equation/value for As(III)
Pseudo-first-order	$\ln(q_e - q_t) = \ln q_e - k_1 t$	$\ln(q_e - q_t) = \ln q_e - k_1 t$
k_1 (min ⁻¹)	-0.003	-0.0068
q_e (mg g ⁻¹)	5.58	1.08
R_1^2	0.634	0.661
Pseudo-second-order	$t/q_t = 1/k_2 q_e^2 + 1/q_e$	$t/q_t = 1/k_2 q_e^2 + 1/q_e$
k_2 (g mg ⁻¹ min ⁻¹)	0.115	0.374
q_e (mg g ⁻¹)	5.31	5.33
R_2^2	0.999	0.999
Intraparticle diffusion	$q_t = k_{id} t^{1/2} + C_i$	$q_t = k_{id} t^{1/2} + C_i$
$K_{id, 1}$	0.38	0.12
C_1	3.2	1.72
R_1^2	0.956	0.966
$K_{id, 2}$	0.2	0.02
C_2	4.04	2.14
R_2^2	0.904	0.962

monolayer coverage, and b is the Langmuir adsorption constant. The plot of $\frac{C_e}{q_e}$ vs. C_e for the sorption gives a straight line of slope $\frac{1}{q_m}$ (Fig. 8).

The linear form of Freundlich isotherm model is represented as

$$\ln q_e = \ln K_F + \frac{1}{n} \ln C_e \quad (6)$$

where K_F and n are the Freundlich constants related to the adsorption capacity and adsorption intensity, respectively; q_e is the equilibrium solute concentration on adsorbent; and C_e is the equilibrium concentration of the solute. According to Eq. (6), the plot of $\ln q_e$ vs. $\ln C_e$ gives a straight line, and K_F and n values can be calculated from the intercept and slope of this straight line (Fig. 9).

Analysis of the experimental data using non-linear equation and linear of Langmuir and Freundlich isotherm showed an opposite result. R^2 was used to measure the strength of the model by determining the closeness of R^2 value to the unity. In this study, the R^2 values of linear analysis for Pb(II) exhibit higher than R^2 values of non-linear analysis for both isotherms. However, a contradicting result is shown for As(III). R^2 values for non-linear analyses for both Langmuir and Freundlich isotherms are higher than linear analysis, hence implying that the Pb(II) is best fitted to linear analysis and As(III) is best fitted to non-linear analysis for both isotherms. In addition, the R^2 values for both isotherms showed that Pb(II) and As(III) fitted well with both isotherms.

The constant parameters (K_F , $1/n$, q_m , and K_L) of isotherms estimated by linear and non-linear expressions were presented in Table 2. Based on the calculation,

Freundlich model showed that theoretical q_e was comparable with experimental q_e because the exponent is between $1 < n < 10$. This trend showed favorable adsorption for Pb(II) and As(III) onto *MNPs-Sp-HEP* adsorbent.

Thermodynamic studies

Thermodynamic parameters including enthalpy changes (ΔH°) and entropy changes (ΔS°) were obtained from Eq. (8), and Gibbs free energy changes (ΔG°) was calculated according to Eq. (7) to study the adsorption behaviors:

$$\Delta G^\circ = -RT \ln K \quad (7)$$

$$\ln K = \frac{\Delta S^\circ}{R} - \frac{\Delta H^\circ}{RT} \quad (8)$$

where K (L/mol) is from Langmuir equation, R is the gas constant (8.314 J/mol K), and T is the temperature in Kelvin. In the plot of $\ln K$ against $1/T$, the ΔH° and ΔS° values are calculated from the slope and intercept of the plot.

The thermodynamic parameters are listed in Table 3. Negative ΔG° values are obtained at different temperature, showing that the adsorption process is possible and spontaneous and required energy from outside of the system. As the temperature increases, the value of ΔG° is decreasing, suggesting that the spontaneous nature of adsorption increases as the temperature goes down.

The negative values of ΔH° , demonstrating the exothermic nature of adsorption and the positive values of ΔS° , suggest that the organization of the adsorbate at the solid-solution interface becomes more random as ion replacement reaction

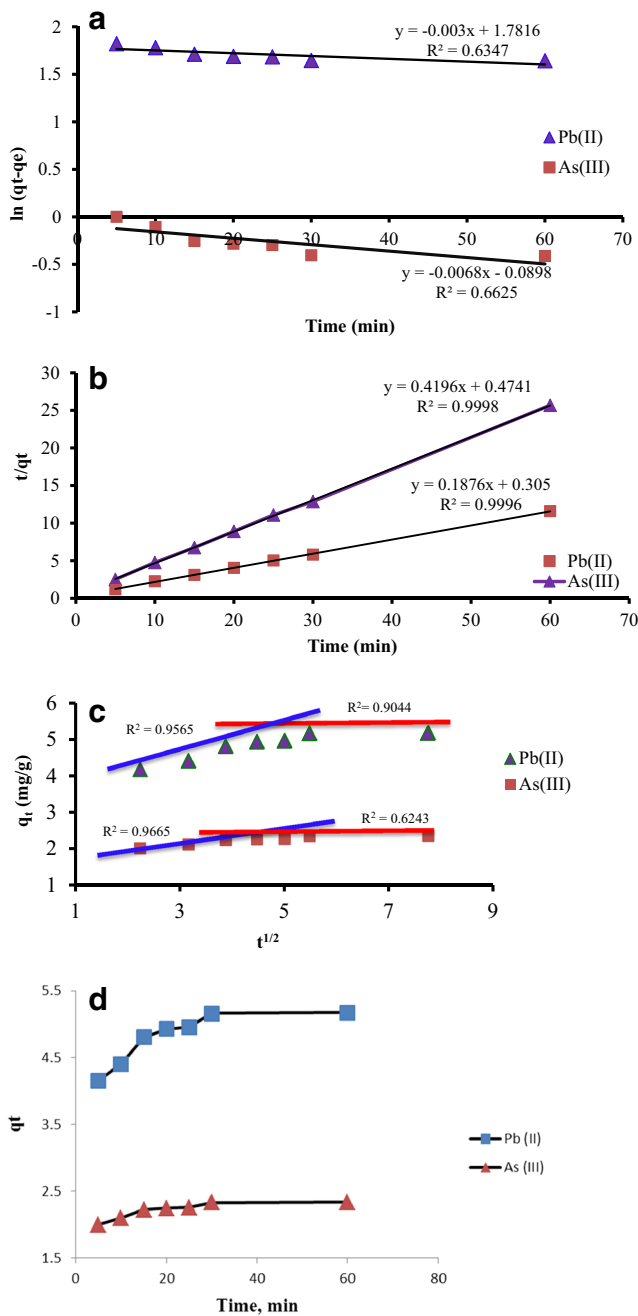


Fig. 10 Pseudo-first-order (a), pseudo-second-order (b), intraparticle diffusion (c), and q_t vs. time for Pb(II) and As(III) ions on immobilized sporopollenin

occurred, while negative values suggest the opposite fact (Daraei et al. 2015; ALOthman et al. 2016).

Adsorption kinetic

Different kinetic models were carried out to study the time required for the adsorption equilibrium to be reached and condition under which there is no variation in adsorption capacity. In this study, the pseudo-first-

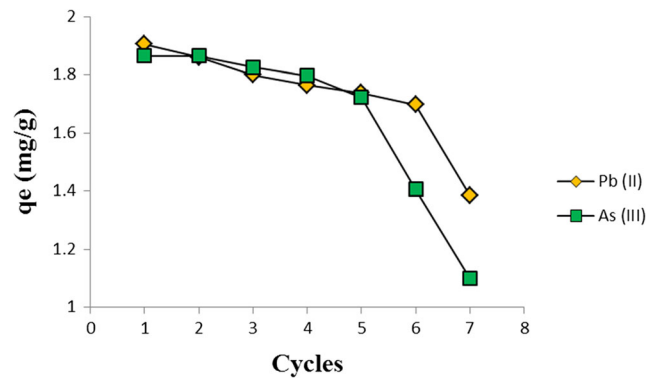


Fig. 11 Seven adsorption-regeneration cycles of Pb(II) and As(III)

order, pseudo-second-order kinetic and intraparticle diffusion models were applied to the kinetic adsorption data to find the best model for the experimental data.

The pseudo-first-order model proposed that as time progresses, the sorbate ions are accumulating over the surface of sorbent (Ho 2006; Daraei et al. 2015).

The pseudo-first-order equation is expressed as

$$\ln(q_e - q_t) = \ln q_e - k_1 t \tag{9}$$

In equation above, q_e and q_t are the amounts of Pb(II) and As(III) ions (mg g^{-1}) adsorbed at equilibrium and at time, t , respectively, and k_1 is the first-order rate constant (min^{-1}). The values of q_e and k_1 were obtained from the linearity of pseudo-first-order rate by plotting $\ln(q_e - q_t)$ vs. time (Fig. 10).

Pseudo-second-order kinetic model which has been applied for analyzing chemisorption kinetics from liquid solutions can be represented by Eq. (10) as follows:

$$\frac{t}{q_1} = \frac{1}{k_2 q_e^2} + \frac{t}{q_e} \tag{10}$$

where k_2 is the rate constant of pseudo-second-order adsorption (g/mg min). The values of k_2 and q_e can be described from the slope and the intercept of the graph t/q_t vs. t , respectively.

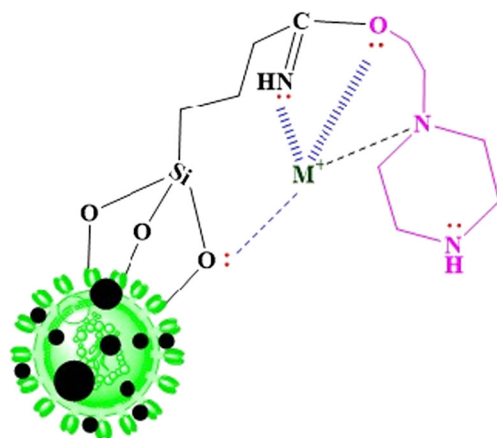


Fig. 12 Proposed mechanism of interaction between metal ions and MNPs-Sp-HEP

By comparing the correlation coefficient (R^2) value from both first-order and second-order kinetics (Table 4), it can be concluded that the experimental data followed pseudo-second-order kinetic and involves chemisorption mechanism (Journal et al. 2010), which revealed that the adsorption process is driven by a chemical reaction occurring at the exposed surface.

Sporopollenin has porous structure; therefore, the adsorption process on porous sorbents was described by intraparticle diffusion, wherein mass transfer within the sorbent particles may involve a short-range diffusion in both the fluid and adsorbed phase (Unlü and Ersoz 2006; Nair et al. 2012). The model is expressed with the equation given by Weber and Morris.

(11)

$$q_t = k_{id}t^{1/2} + C_i$$

where q_t and k_{id} are the amount of metal ions adsorbed at time t and intraparticle diffusion rate constant, respectively, whereas C_i is the intercept which gives the idea about the thickness of the boundary layer. Intraparticle diffusion values (Table 4) were obtained from linearity of q_t vs. $t^{1/2}$ plot. Figure 10c shows two-part linearity; i.e., mass transfer (first stage) and equilibrium part (second stage) for intraparticle diffusion model revealed that Pb(II) and As(III) ion adsorption was conducted in two separate regions with two straight lines. First part with a sharp slope showed that the adsorption rate is fast and adsorption is favorable on the surface. The second part with slow slope shows that the adsorption rate is slow and intraparticle diffusion is not involved in adsorption (Nodeh et al. 2015).

Regeneration of *MNPs-Sp-HEP*

The restoration of adsorption capability is a crucial factor in practical application of the adsorbent. The adsorption of heavy metals observed on *MNPs-Sp-HEP* at low pH implies that acid treatment is a feasible approach to regenerating the heavy metal-loaded adsorbent.

Due to the stability of *MNPs-Sp-HEP* under acidic conditions, Pb- and As-loaded adsorbent was regenerated using 0.1 M HNO_3 solution and the regeneration adsorbent was reused in adsorption in seven consecutive cycles. Adsorption efficiency of the regenerated adsorbents was shown in Fig. 11. The adsorption capacity had decreased slightly by first five adsorption-regeneration capacity cycles, and drastically dropped at cycles 5 and 6 for As(III) and Pb(II), respectively. This is might be due to the partial breakup of outer *MNPs-Sp-HEP* shell and cell walls at high concentration of nitric acid (Şener et al. 2014).

Mechanism

The adsorption mechanism of Pb(II) and As(III) metal ions on *MNPs-Sp-HEP* was explained in Fig. 9. Pb(II) and As(III) metal ion adsorption mechanism for the *MNPs-Sp-HEP* adsorbent is highly pH dependent and can be explain as follows: since *MNPs-Sp-HEP* contains nitrogen and oxygen groups, these N and O groups are highly electronegative due to the abundance of free lone pair of electrons. These lone pair electrons shows binding abilities toward the Pb(II) and As(III) cation as represented in Fig. 12.

Conclusion

The magnetic sporopollenin-functionalized 1-(2-hydroxyethyl) piperazine was successfully synthesized, characterized, and employed as an promising adsorbent for the removal of Pb(II) and As(III) ions from aqueous solution prior to ICP determination. The *MNPs-Sp-HEP* is suitable for extraction operation as it provides outstanding magnetically separation, stabilization in aqueous sample, and quick process. Adsorption experimental data of Pb(II) and As(III) fitted well with both isotherms. Kinetic model performed that the adsorption rate was controlled by pseudo-second-order. Thermodynamic study showed that Pb(II) and As(III) adsorption on *MNPs-Sp-HEP* are spontaneous and exothermic process due to negative energy of $-\Delta G$ and $-\Delta H$, respectively. The positive value of ΔS shows that the organization of adsorbate at the solid/solution interfaces becomes more random. The chelating effect of *MNPs-Sp-HEP* increased to the sorption of heavy metal ions compared to raw sporopollenin. Overall, it can be concluded that the proposed sorbent system is practical and efficient for the removal of heavy metals from aqueous environment with advantages of being inexpensive and largely available.

Acknowledgments The authors would like to thank the University of Malaya for the financial support through the grants PG049-2015B, RP011B-14SUS, and RP020A-16SUS.

References

- Aguado J, Arsuaga JM, Arencibia A et al (2009) Aqueous heavy metals removal by adsorption on amine-functionalized mesoporous silica. *J Hazard Mater* 163:213–221. doi:10.1016/j.jhazmat.2008.06.080
- Ali I (2012) New generation adsorbents for water treatment. *Chem Rev* 112:5073–5091
- ALothman ZA, Habila MA, Al-Shalan NH et al (2016) Adsorptive removal of Cu(II) and Pb(II) onto mixed-waste activated carbon: kinetic, thermodynamic, and competitive studies and application to real wastewater samples. *Arab J Geosci* 9:315. doi:10.1007/s12517-016-2350-9

- Arora V, Sood A, Shah J, et al (2016) Synthesis and characterization of thiolated pectin stabilized gold coated magnetic nanoparticles. *Mater Chem Phys* 1–7. doi: [10.1016/j.matchemphys.2016.01.056](https://doi.org/10.1016/j.matchemphys.2016.01.056)
- Baharin SNA, Muhamad Sarih N, Mohamad S et al (2016) Removal of endocrine disruptor di-(2-ethylhexyl)phthalate by modified polythiophene-coated magnetic nanoparticles: characterization, adsorption isotherm, kinetic study, thermodynamics. *RSC Adv* 6: 44655–44667. doi:[10.1039/C6RA04172H](https://doi.org/10.1039/C6RA04172H)
- Bakhshaei S, Kamboh MA, Nodeh HR et al (2016) RSC advances aromatic hydrocarbons and chlorophenols based nanoparticles and their determination by. *RSC Adv* 6:77047–77058. doi:[10.1039/C6RA13702D](https://doi.org/10.1039/C6RA13702D)
- Barakat MA (2011) New trends in removing heavy metals from industrial wastewater. *Arab J Chem* 4:361–377. doi:[10.1016/j.arabjc.2010.07.019](https://doi.org/10.1016/j.arabjc.2010.07.019)
- Binks BP, Boa AN, Kibble MA et al (2011) Sporopollenin capsules at fluid interfaces: particle-stabilised emulsions and liquid marbles. *Soft Matter* 7:4017. doi:[10.1039/c0sm01516d](https://doi.org/10.1039/c0sm01516d)
- Cheng Y, Yang C, He H et al (2015) Biosorption of Pb(II) ions from aqueous solutions by waste biomass from biotrickling filters: kinetics, isotherms, and thermodynamics. *J Environ Eng*:1–7. doi:[10.1061/\(ASCE\)EE.1943-7870.0000956](https://doi.org/10.1061/(ASCE)EE.1943-7870.0000956)
- Chou WL, Wang CT, Huang KY, Liu TC (2011) Electrochemical removal of salicylic acid from aqueous solutions using aluminum electrodes. *Desalination* 271:55–61. doi:[10.1016/j.desal.2010.12.013](https://doi.org/10.1016/j.desal.2010.12.013)
- Çimen A, Bilgiç A, Kursunlu AN, Gübbük İH (2014) Adsorptive removal of Co(II), Ni(II), and Cu(II) ions from aqueous media using chemically modified sporopollenin of *Lycopodium clavatum* as novel biosorbent. *Desalin Water Treat*. doi:[10.1080/19443994.2013.806228](https://doi.org/10.1080/19443994.2013.806228)
- Community E (1998) Council Directive 98/83/EC of 3 November 1998 on the quality of water intended for human consumption. *Off J Eur Communities* L330:32–54
- Dabrowski A, Hubicki Z, Podkoscielny P, Robens E (2004) Selective removal of the heavy metal ions from waters and industrial wastewaters by ion-exchange method. *Chemosphere* 56:91–106. doi:[10.1016/j.chemosphere.2004.03.006](https://doi.org/10.1016/j.chemosphere.2004.03.006)
- Daraei H, Mittal A, Noorisepehr M, Mittal J (2015) Separation of chromium from water samples using eggshell powder as a low-cost sorbent: kinetic and thermodynamic studies. *Desalin Water Treat* 53:214–220. doi:[10.1080/19443994.2013.837011](https://doi.org/10.1080/19443994.2013.837011)
- Dyab AKF, Abdallah EM, Ahmed SA, Rabee MM (2016) Fabrication and characterisation of novel natural *Lycopodium clavatum* sporopollenin microcapsules loaded in-situ with nano-magnetic humic acid-metal complexes Retrieved 6 April 2017, from http://file.scirp.org/pdf/JEAS_2016112417465025.pdf
- Edition F (2011) Guidelines for drinking-water quality. *WHO Chron* 38: 104–108
- Fadzil F, Ibrahim S, Hanafiah MAKM (2016) Adsorption of lead(II) onto organic acid modified rubber leaf powder: batch and column studies. *Process Saf Environ Prot* 100:1–8. doi:[10.1016/j.psep.2015.12.001](https://doi.org/10.1016/j.psep.2015.12.001)
- Georgiou Y, Mouzourakis E, Bourlinos AB et al (2016) Surface decoration of amine-rich carbon nitride with iron nanoparticles for arsenite (As III) uptake: the evolution of the Fe-phases under ambient conditions. *J Hazard Mater* 312:243–253
- Gohari RJ, Lau WJ, Matsuura T, Ismail AF (2013) Fabrication and characterization of novel PES/Fe–Mn binary oxide UF mixed matrix membrane for adsorptive removal of As(III) from contaminated water solution. *Sep Purif Technol* 118:64–72
- Gupta VK, Rastogi A (2008) Biosorption of lead from aqueous solutions by green algae *spirogyra* species: kinetics and equilibrium studies. *J Hazard Mater* 152:407–414. doi:[10.1016/j.jhazmat.2007.07.028](https://doi.org/10.1016/j.jhazmat.2007.07.028)
- He Z (2015) Heavy metal contamination of soils: sources, indicators, and assessment. *J Environ Indic* 9:17–18
- Ho YS (2006) Isotherms for the sorption of lead onto peat: comparison of linear and non-linear methods. *Polish J Environ Stud* 15:81–86. doi: [10.1016/j.watres.2005.10.040](https://doi.org/10.1016/j.watres.2005.10.040)
- Ibrahim WAW, Nodeh HR, Aboul-Enein HY, Sanagi MMS (2015a) Magnetic solid-phase extraction based on modified ferum oxides for enrichment, preconcentration, and isolation of pesticides and selected pollutants. *Crit Rev Anal Chem* 45:270–287. doi:[10.1080/10408347.2014.938148](https://doi.org/10.1080/10408347.2014.938148)
- Ibrahim WA, Nodeh HR, Sanagi MM (2015b) Graphene-based materials as solid phase extraction sorbent for trace metal ions, organic compounds and biological sample preparation. *Crit Rev Anal Chem* 46: 267–83. doi:[10.1080/10408347.2015.1034354](https://doi.org/10.1080/10408347.2015.1034354)
- Jain M, Garg V, Kadirvelu K, Sillanpää M (2015) Adsorption of heavy metals from multi-metal aqueous solution by sunflower plant biomass-based carbons. *Int J Environ Sci* doi. doi:[10.1007/s13762-015-0855-5](https://doi.org/10.1007/s13762-015-0855-5)
- Journal B, Kumar PS, Vincent C et al (2010) Kinetics and equilibrium studies of Pb²⁺ ion removal from aqueous solutions by use of nano-silver sol-coated activated carbon. *Brazilian J Chem Eng* 27:339–346
- Kamboh MA, Yilmaz M (2013) Synthesis of N-methylglucamine functionalized calix[4]arene based magnetic sporopollenin for the removal of boron from aqueous environment. *Desalination* 310:67–74. doi:[10.1016/j.desal.2012.10.034](https://doi.org/10.1016/j.desal.2012.10.034)
- Kamboh MA, Ibrahim WAW, Nodeh HR et al (2016) The removal of organophosphorus pesticides from water using a new amino-substituted calixarene-based magnetic sporopollenin. *New J Chem* 40:3130–3138. doi:[10.1039/C5NJ02284C](https://doi.org/10.1039/C5NJ02284C)
- Lapwanit S, Trakulsujaritchock T, Nongkhai PN (2016) Chelating magnetic copolymer composite modified by click reaction for removal of heavy metal ions from aqueous solution. *Chem Eng J* 289:286–295. doi:[10.1016/j.cej.2015.12.073](https://doi.org/10.1016/j.cej.2015.12.073)
- Liu Q-S, Zheng T, Wang P et al (2010) Adsorption isotherm, kinetic and mechanism studies of some substituted phenols on activated carbon fibers. *Chem Eng J* 157:348–356. doi:[10.1016/j.cej.2009.11.013](https://doi.org/10.1016/j.cej.2009.11.013)
- Meenakumari M, Philip D (2015) Degradation of environment pollutant dyes using phytosynthesized metal nanocatalysts. *Spectrochim Acta - Part A Mol Biomol Spectrosc* 135:632–638. doi:[10.1016/j.saa.2014.07.037](https://doi.org/10.1016/j.saa.2014.07.037)
- Nair DG, Hansdah K, Dhal B et al (2012) Bioremoval of chromium(III) from model tanning effluent by novel microbial isolate. *Int J Metall Eng* 1:12–16. doi:[10.5923/j.ijmee.20120102.01](https://doi.org/10.5923/j.ijmee.20120102.01)
- Nodeh H, Wan Ibrahim W, Sanagi M (2015) Magnetic graphene oxide as adsorbent for the removal of lead(II) from water samples. *Jurnal Teknologi* 78(3–2):25–30
- Nonkumwong J, Ananta S, Srisombat L (2016) Effective removal of lead(II) from wastewater by amine-functionalized magnesium ferrite nanoparticles. *RSC Adv* 6:47382–47393
- Paunov VN, Stoyanov SD (2007) Sporopollenin micro-reactors for in-situ preparation, encapsulation and targeted delivery of active components. *J Mater Chem* 17:609–612. doi:[10.1039/b615865j](https://doi.org/10.1039/b615865j)
- Sáez C, de Vidales MJM, Cañizares P et al (2014) Irradiated electrochemical processes for the removal of persistent organic pollutants from waters and wastewaters. *Chem Eng Trans* 41:103–108. doi:[10.3303/CET1441018](https://doi.org/10.3303/CET1441018)
- Şener M, Reddy DHK, Kayan B (2014) Biosorption properties of pretreated sporopollenin biomass for lead(II) and copper(II): application of response surface methodology. *Ecol Eng* 68:200–208. doi: [10.1016/j.ecoleng.2014.03.024](https://doi.org/10.1016/j.ecoleng.2014.03.024)
- Şener M, Kayan B, Akay S, Gözmen B (2016) Fe-modified sporopollenin as a composite biosorbent for the removal of Pb²⁺ from aqueous solutions. *Desalin Water Treat*. doi:[10.1080/19443994.2016.1182449](https://doi.org/10.1080/19443994.2016.1182449)
- Shahabuddin S, Sarih NM, Afzal Kamboh M et al (2016) Synthesis of polyaniline coated graphene oxide @ SrTiO₃ nanocube

- nanocomposites for enhanced removal of carcinogenic dyes from aqueous solution. *Sciprints*. doi:[10.20944/preprints201608.0128.v1](https://doi.org/10.20944/preprints201608.0128.v1)
- Sivashankar R, Sathya AB, Vasantharaj K, Sivasubramanian V (2014) Magnetic composite an environmental super adsorbent for dye sequestration—a review. *Environ Nanotechnol, Monit Manag* 1–2: 36–49. doi:[10.1016/j.enmm.2014.06.001](https://doi.org/10.1016/j.enmm.2014.06.001)
- Sureshkumar V, Daniel SCGK (2016) Fabrication of chitosan–magnetite nanocomposite strip for chromium removal. *Appl Nanosci*:277–285. doi:[10.1007/s13204-015-0429-3](https://doi.org/10.1007/s13204-015-0429-3)
- Swamalatha K, Ayoob S (2016) Adsorption studies on coir pith for heavy metal removal. *Int J Sustain Eng* 7038:1–7. doi:[10.1080/19397038.2016.1152323](https://doi.org/10.1080/19397038.2016.1152323)
- Tang W, Su Y, Li Q et al (2013) Superparamagnetic magnesium ferrite nanoadsorbent for effective arsenic (III, V) removal and easy magnetic separation. *Water Res* 47:3624–3634. doi:[10.1016/j.watres.2013.04.023](https://doi.org/10.1016/j.watres.2013.04.023)
- Tyrovola K, Peroulaki E, Nikolaidis NP (2007) Modeling of arsenic immobilization by zero valent iron. *Eur J Soil Biol* 43:356–367
- Ucar S, Erdem M, Tay T, Karagöz S (2014) Removal of lead(II) and nickel(II) ions from aqueous solution using activated carbon prepared from rapeseed oil cake by Na₂CO₃ activation. *Clean Technol Environ Policy* 747–756. doi: [10.1007/s10098-014-0830-8](https://doi.org/10.1007/s10098-014-0830-8)
- Unlü N, Ersoz M (2006) Adsorption characteristics of heavy metal ions onto a low cost biopolymeric sorbent from aqueous solutions. *J Hazard Mater* 136:272–280. doi:[10.1016/j.jhazmat.2005.12.013](https://doi.org/10.1016/j.jhazmat.2005.12.013)
- Vilela D, Parmar J, Zeng Y, et al (2016) Graphene based microbots for toxic heavy metal removal and recovery from water. *Nano Lett acs. Nanolett.* 6b00768. doi:[10.1021/acs.nanolett.6b00768](https://doi.org/10.1021/acs.nanolett.6b00768)
- Vymazal J, Brezinova T (2015) The use of constructed wetlands for removal of pesticides from agricultural runoff and drainage: a review. *Environ Int* 75:11–20. doi:[10.1016/j.envint.2014.10.026](https://doi.org/10.1016/j.envint.2014.10.026)
- WHO (2008) Guidelines for drinking-water quality: incorporating first and second addenda to third edition. *Theatr Rec* 1:1–494
- Zheng X, He L, Duan Y et al (2014) Poly(ionic liquid) immobilized magnetic nanoparticles as new adsorbent for extraction and enrichment of organophosphorus pesticides from tea drinks. *J Chromatogr A* 1358:39–45. doi:[10.1016/j.chroma.2014.06.078](https://doi.org/10.1016/j.chroma.2014.06.078)